Available online at www.sciencedirect.com

ScienceDirect

Geochimica et Cosmochimica Acta 120 (2013) 239–250

Geochimica et Cosmochimica Acta

www.elsevier.com/locate/gca

Siderophile element partitioning between cohenite and liquid in the Fe–Ni–S–C system and implications for geochemistry of planetary cores and mantles

Antonio S. Buono [a,*], Rajdeep Dasgupta [b], Cin-Ty A. Lee [b], David Walker [a]

[a] Lamont Doherty Earth Observatory, Department of Earth and Environmental Sciences, Columbia University, Palisades, NY 10964, USA
[b] Rice University, Department of Earth Science, MS 126, 6100 Main Street, Houston, TX 77005, USA

Received 2 March 2012; accepted in revised form 20 June 2013; Available online 4 July 2013

Abstract

We experimentally investigated the effects of pressure and S content on partition coefficients (D) between crystalline cohenite and liquid in the Fe–Ni–S–C system. Compositions with S contents of 0, 4.72, and 14.15 wt.%, in an Fe-rich mix containing a constant C (4.72 wt.%), Ni (5.23 wt.%), and W, Re, Os, Pt, and Co (totaling 0.43 wt.%) were equilibrated at 1150 °C and 3 and 6 GPa. Our cohenite–melt D data are compared to literature Fe–Ni–S and Fe–Ni–C experiments involving a crystalline phase of Fe. There is a change in D when the solid is cohenite rather than crystalline iron. Compared to solid-Fe/melt Ds, cohenite/melt Ds are lower for all elements except W.

The light element (S + C) content of the liquid influences partitioning between cohenite and liquid as it also does between crystalline Fe and liquid. The controls are similar but not identical. In the cohenite-bearing experiments, D_{Ni} decreases as S + C increases. Ni is excluded from the crystallizing solid if the solid is cohenite. And yet, in the Fe–Ni–S–C system, cohenite is stable to higher P than in the Fe–S–C system. As in the Fe-metallic liquid systems the non-metal avoidance principle of Jones and Malvin (1990) is applicable to the Fe_3C-metallic liquid system studied here.

Carbon in the mantle is expected to combine with neutral Fe to replace metal with cohenite. In which case, the budget of highly siderophile elements is likely to be accommodated by Fe–Ni–S–C liquids once they form upon incipient melting because most Ds for cohenite/liquid are <1 in this system. The crystallization of cohenite from such liquids in Earth's core is unlikely to improve the case for core–mantle interaction based on Pt–Re–Os systematics.

1. INTRODUCTION

During planetary formation, metals and silicates separate. This separation leads to planetary stratification into the core and mantle. As the planet cools, the core (a metallic-rich liquid) begins to solidify. This solidification changes the composition of the liquid as the crystals grow. Fractionation of light and siderophile elements is key to track such inner core crystallization process for evolution of outer core and possible core–mantle interaction (e.g., Walker, 2000; Buffett et al., 2000; Buffett, 2003; Brandon et al., 1998; Brandon and Walker, 2005; Van Orman et al., 2008). Similarly, the presence of a small amount of Fe-rich metallic phase in the silicate mantle is also thought to be important for siderophile element inventory of the bulk mantle (e.g., Newsom and Sims, 1991; Frost et al., 2004; Rohrbach et al., 2007). The impact of carbon and sulfur upon siderophile element storage and distribution in Fe-rich mantle metal has yet to be emphasized and constrained.

The core of the Earth, and probably other planetary bodies, needs to contain one or more light elements to fulfill density requirements (Birch, 1952; Labrosse, 2003). The

* Corresponding author. Address: 505 Del Norte Street, Houston, TX 77018, USA. Tel.: +1 812 360 3361.
E-mail address: antonio.buono@gmail.com (A.S. Buono).

0016-7037/$ - see front matter © 2013 Elsevier Ltd. All rights reserved.
http://dx.doi.org/10.1016/j.gca.2013.06.024

Earth requires that 5–10% of its core be composed of elements lighter than Fe–Ni (Birch, 1952; Poirier, 1994; Anderson and Isaak, 2002; McDonough, 2003). For an element to be a major core component it must have high cosmic abundances and be compatible with Fe. There are five plausible elements that can fill this role: H, O, C, S, and Si. The only planetary cores that we can study in hand specimen are those of remnant planets, in the form of iron meteorites. The most abundant light elements in these cores are S and C. Carbon occurs in abundances up to 2 wt.% and $(Fe,Ni)_3C$ (cohenite) is an accessory phase in iron meteorites (Buchwald, 1975). C is 8 times more abundant in the solar system than Fe but is often ignored as a core component because of its volatility and the difficulty of measuring it in samples. If the core of a planet forms at an elevated pressure then the volatility driven loss of C can be avoided owing to higher solubility of C in deep Earth phases, especially in metallic systems.

Addition of C to an Fe-rich core can stabilize an Fe-carbide. This carbide is likely either cohenite or Fe_7C_3. Recent work (Lord et al., 2009), has argued that there is an invariant point along the Fe-saturated solidus terminating cohenite to Fe_7C_3 + liquid at 120 GPa. If this is the case, cohenite's importance as an inner core material may be restricted to smaller planetary bodies, such as Earth's Moon and Mercury where the inner pressures are as low as 4–8 GPa, but for Earth the carbide phase of interest is Fe_7C_3. However, the solidus boundary between cohenite and Fe + Fe_7C_3 (Lord et al., 2009) is not well constrained, indicating that cohenite could still be a stable phase at CMB pressures. Even though there is the possibility of cohenite being a stable phase, there are several reasons that the inner core of the Earth is primarily Fe metal and not cohenite. First, the density of cohenite at Earth's core pressures is too low (Ono and Mibe, 2010). Second, Pb isotopic age of the Earth supports the conclusion reached through mass balance that the Earth's core C content is probably no more than 0.25 wt.% (Dasgupta and Walker, 2008; Wood and Halliday, 2010). Finally, recent experiments, which constrained carbon partitioning between core-forming metallic liquid and silicate liquid also suggest that equilibrium core formation likely resulted in a bulk core with 0.20–0.25 wt.% carbon (Dasgupta et al., 2013). Currently the amount of C which can be incorporated into metallic Fe at core conditions is unconstrained. Using 0.25 wt.% as the most likely C content of the Earth's core would result in a maximum of only 4 wt.% cohenite if C was fully excluded from Fe metal. While the presence of cohenite in the Earth's core remains an open question, its presence in the Earth's mantle may be unavoidable.

Gradual disproportionation of the mantle assemblage with depth in Earth's high pressure environment to give Fe metal and Fe^{3+}-bearing phases suggests that Earth's mantle might be metal saturated at depths in excess of 250 km and as much as 0.1–1.0 wt.% metallic Fe (or Fe–Ni alloy) could be present (Frost et al., 2004; Rohrbach et al., 2007, 2011). This, in addition to the equilibrium presence of reduced carbon such as diamond and graphite, may lead to the formation of Fe-rich carbides, cohenite and Fe_7C_3 at mantle depths (Dasgupta and Hirschmann, 2010; Dasgupta, 2013). Moreover, as sulfur in the mantle is present almost entirely as sulfide, equilibrium phase relations and siderophile element geochemistry of the Fe–(±Ni)–C±S system become relevant. The finding of cohenite, troilite, and metallic-Fe as inclusions in mantle-derived garnet (Jacob et al., 2004) validates such a hypothesis. Comparison of average sub-ridge mantle adiabats with the extrapolation of near-liquidus phase diagram of Fe–(±Ni)–C±S system (Dasgupta et al., 2009) suggests that Fe-rich carbide and Fe–Ni–C–S liquid may coexist in the Earth's mantle over a large depth range. Hence the knowledge of siderophile element partitioning between cohenite and Fe–C–S liquid is important for knowing the contribution of various phases in siderophile element budget of the mantle.

For phase relations and siderophile element partitioning in light element bearing metallic systems, previous studies have focused on a Fe-rich binary systems with Fe-alloy being the solid phase of interest (Wood, 1993; Chabot et al., 2006, 2007, 2008; Van Orman et al., 2008; Lord et al., 2009; Stewart et al., 2009; Walker et al., 2009; Buono and Walker, 2011), but the effects of the crystallization of carbide on partitioning in a multi-component system have yet to be looked at in detail.

In this paper, we examine partitioning of some key siderophile elements in the Fe–Ni–S–C system, with variable S content, at 3 and 6 GPa at 1150 °C. Cohenite is a stable phase in the Fe–Ni–C–S system at this temperature at both 3 and 6 GPa, removing the complexity that a variety of carbide solids could add. The Fe–Ni–S–C chemical system was chosen because S is known to readily alloy with Fe, though its solubility decreases with increasing pressure. S also has a large impact on the melting point of Fe (Brett and Bell, 1969; Usselman, 1975; Fei et al., 1997; Morard et al., 2007; Chen et al., 2008; Buono and Walker, 2011) which decreases the required core temperatures to sustain a dynamo. Large changes in P and T must be taken into account when talking about planetary cores. Partition coefficients are often assumed to be independent of intensive variables such as temperature, pressure, oxygen fugacity, and phase compositions (Bild and Drake, 1978). However, there is a growing recognition that it is important to constrain the control of these intensive variables on a given partition coefficient. In this paper, we look at 3 of these variables that might affect partition coefficients in metallic crystal–liquid assemblages; the effect of S on partitioning in the Fe–Ni–C system; the effect of P on partitioning in the Fe–Ni–C and Fe–Ni–C–S systems; and how changing the solid from metallic-Fe to Fe-carbide affects D. Our choice of siderophile trace elements Ni, Co, W, Re, Os, and Pt for study was conditioned by the relatively large data base for the first 3 elements that exists for metal/liquid partitioning. The second 3 elements chosen are the key siderophile elements for understanding Os isotope evolution in the Earth's core (Brandon and Walker, 2005; Walker et al., 2005). We wished to revisit the issue of Pt–Re–Os behavior in a C-bearing liquid metal system for evidence of behavior change introduced by carbon.

2. EXPERIMENTAL AND ANALYTICAL METHODS

2.1. Starting materials

Experimental starting materials were prepared by mixing Fe, synthetic FeS, and diamond powder with metallic powders that comprised the trace component. Sources for these materials were: Fe (99.9% Fe powder from Alfa-Aesar), synthesized FeS (mixture of 99.9% Fe powder (Alfa-Aesar) with S (Fisher Scientific)), and diamond powder (1–5 μm, Warren Diamond Powder Co.). The FeS was synthesized by mixing sulfur and iron powder in equimolar proportions and then by sealing the mix in an evacuated silica tube. The silica tube was then heated to 1000 °C for 1 h to aid reaction in the mixture. The resulting powder was then ground and mixed with the desired proportion of iron, diamond, and trace component powder in an agate mortar, under acetone.

Because we wanted to see the effect of varying S, we created three starting materials with different proportions. These blends are reported in Table 1. In all materials, the trace component consists of 0.09–0.08 wt.% of each of W, Co, Re, Os, and Pt. These mixes were incompletely homogenized so there is some variability in the initial trace element content of the starting material. Throughout this paper, the composition of the starting material will be referred to by wt.% S. After mixing and drying, all the starting mixes were stored in stoppered vials in a glass desiccator.

2.2. Experimental design and procedure

Experiments were performed using a Walker-style multi-anvil apparatus at the Lamont Doherty Earth Observatory. Initial, reconnaissance experiments were performed over a pressure and temperature range of 3–6 GPa and 1150–1450 °C (Appendix 1). To isolate the effect of pressure on siderophile element partitioning, all the experiments, for which trace elements were measured, were carried out at 1150 °C. Experiments used castable $MgO–Al_2O_3–SiO_2$ octahedral assemblies, $LaCrO_3$ furnaces, crushable MgO spacers and capsules, and 8 mm truncation edge length (TEL) WC cubes as anvils to exert pressure onto the sample assembly. A force of 300 tons was used to achieve 6 GPa of sample pressure and 150 tons for 3 GPa. Type-D W/Re thermocouples were used to monitor and control temperature during the experiments and were inserted laterally through the gasket fins of the castable octahedra.

All experiments were pressurized cold and held at a temperature of 800 °C for 16–24 h (Table 1). This minimized porosity in the capsules, to prevent seepage when the temperature was raised and the metals melted. After sintering, experiments were heated at an average rate of 200 °C/min to 1400 °C, and held for at least 30 min to homogenize the C. The temperature for all cohenite–liquid experiments was then lowered to 1150 °C in about a minute and held for 18–26 h (Table 1), a significantly longer duration than previous studies in similar systems (Chabot et al., 2008), to help ensure equilibration. Experiments were quenched by terminating power to the heater. At the end of the experiment, the assembly was gradually decompressed and the recovered assemblies were mounted in epoxy for sample preparation and analysis. The assemblies were ground longitudinally to expose the medial section of the samples. Coarse sample grinding was done using a silicon carbide strip grinder and fine polishing with 0.3 μm Al_2O_3 powder on a lapidary wheel. Water was used as lubricant during

Table 1
Experimental conditions, phase assemblage, and phase proportions in run product.

Run no.	P (GPa)	T (°C)	Duration (h)	Homogenization T (°C)	Homogenization time (min)	Bulk composition of the starting material	Phase assemblage and proportion	$\sum r^{2a}$
TT-731	3	1150	23.38	1400	60	89.62 wt.% Fe; 4.72 wt.% C; 5.23 wt.% Ni; 0.43 wt.% Trace; 0% S	72% Liquid + 28% Cohenite	0.1
TT-716	6	1150	18.87	1400	188	89.62 wt.% Fe; 4.72 wt.% C; 5.23 wt.% Ni; 0.43 wt.% Trace; 0% S	53% Liquid + 47% Cohenite	5.7
TT-733	3	1150	20.58	1400	60	84.9 wt.% Fe; 4.72 wt.% C; 4.72 wt.% S; 5.23 wt.% Ni; 0.43 wt.% Trace	22% S-rich Liquid + 31% Cohenite + 47% Unreacted, disequilibrium phase	0
TT-726	6	1150	26.07	1400	62	84.9 wt.% Fe; 4.72 wt.% C; 4.72 wt.% S; 5.23 wt.% Ni; 0.43 wt.% Trace	28% Liquid + 72% Cohenite	6.9
TT-728	3	1150	21.72	1400	65	75.47 wt.% Fe; 4.72 wt.% C; 14.15 wt.% S; 5.23 wt.% Ni; 0.43 wt.% Trace	60% Liquid + 40% Cohenite	1.4
BB-965	6	1150	22.22	1400	30	75.47 wt.% Fe; 4.72 wt.% C; 14.15 wt.% S; 5.23 wt.% Ni; 0.43 wt.% Trace	65% Liquid + 35% Cohenite + Trace Graphite	2.6

All the experiments were conducted in MgO capsules. Phase assemblage and proportion was calculated based on the bulk and final compositions, assuming no loss during the runs. The no loss assumption is based on the use of an MgO capsule and no apparent leakage observed in microprobe imaging.

Average uncertainty in temperature is ±25 °C. All experiments are arranged according to increasing S content of the starting mixes.

[a] '$\sum r^2$' is the sum of the squares of the residuals from the phase assemblage calculation.

polishing. After a polished surface was achieved, samples and standards were cleaned in an ultrasonic bath and coated with Al for characterization of C content with an electron microprobe. Samples were then re-polished and coated with C for further characterization with an electron microprobe. After chemical analyses using electron microprobe were completed, carbon-coating was removed and samples were analyzed using LA-ICP-MS.

2.3. Analysis of the run products

2.3.1. EPMA analysis with Al coating

Samples were imaged and analyzed for Fe, Ni, S, and C using a Cameca SX100 electron probe microanalyzer (EPMA) at the American Museum of Natural History. Fe-wire, Ni-wire, natural troilite, and experimentally synthesized stoichiometric cohenite were used as primary analytical standards. The samples and the standards were Al coated simultaneously for each run to keep X-ray absorptions uniform. For Wavelength Dispersive Spectrometry (WDS) analysis of C, a Ni/C multilayer crystal (LPC2: large PC2 with $2d$ spacing = 9.5 nm) was used, following the analytical protocol of Dasgupta and Walker (2008). An accelerating voltage of 10 kV and a probe current of 70–100 nA was used for all the analyses. For the bulk of the analyses, fully focused beam with a 30×30 μm raster was used for quenched melt and crystalline domains. Quenched melt pools in a limited number of experiments were analyzed using a fully focused beam with a 15×15 μm raster. Counting time was 20 s on peak and 10 s on each background for Fe, Ni, and S. To avoid contamination-induced gain, C was measured for 10 s on peak and 5 s on each background.

2.3.2. EPMA analysis with C coating

Samples were imaged and analyzed for Fe, Ni, and S using a Cameca SX100 EPMA at the American Museum of Natural History. Natural troilite, Fe-wire, and Ni-wire were used as primary analytical standards for the major elements. S, Fe, and Ni were analyzed using the LPET and LLIF crystals with an accelerating voltage of 15 keV and a probe current of 20 nA with a peak time of 20 s.

For the bulk of the analyses, fully focused beam with a 30×30 μm raster was used for quenched melt and crystalline domains. Quenched melt pools in a limited number of experiments were analyzed using a fully focused beam with a 15×15 μm raster.

2.3.3. LA-ICP-MS analysis

Analyses of Fe, Ni, and trace elements (Fe, Ni, Co, W, Re, Os, and Pt) were done by laser ablation inductively coupled plasma mass spectrometry (LA-ICP-MS) at Rice University using a ThermoFinnigan Element 2 ICP-MS coupled to a New Wave 213 nm laser ablation system (Agranier and Lee, 2007). Analyses were performed in medium mass resolution ($m/\Delta m = 3500$) in order to resolve all major molecular interferences (which affect in particular Fe, Co, and Ni). The following isotopes were measured during analysis: ^{57}Fe, ^{59}Co, ^{61}Ni, ^{182}W, ^{183}W, ^{185}Re, ^{190}Os, ^{192}Os, ^{194}Pt, and ^{195}Pt. The laser was set at 10 Hz pulse frequency and an energy density of 9–11 J/cm^2. Measurements consisted of about 10 analyses of gas flow background followed by 40–50 measurements of the ablation signal. Gas background was averaged and then subtracted from the ablation signal. Background-corrected signals were converted to concentrations using a combination of internal and external standards. ^{57}Fe was used as an internal standard for both metal carbide crystals and quenched metallic liquids. Hoba iron meteorite was used as a primary external standard while iron meteorite Filomena was used as secondary external standard (Campbell and Humayun, 2005). For each experiment, the locations to be analyzed were selected from a BSE or optical images of the sample and typically laser spot size of 40 μm was used for crystals and 110 μm for quenched melt pools. Reported errors in Table 2 were calculated as twice the standard error of the mean of the replicate analyses of each phase. The measured isotopic compositions of W, Os, and Pt were identical to natural isotopic compositions to within error, indicating that interferences were not an issue. For a given element, concentrations determined using each isotope was also identical, so the average of the two is reported in Table 2.

3. RESULTS

The experimental conditions, resulting phase assemblages, and compositions are documented in Tables 1 and 2. The textures of the experimental charges are shown in Fig. 1. All discussions about Ds for Co, Os, Pt, Re, and W (Table 3) refer to the LA-ICP-MS data where Fe was used as the internal standard. The phases present and phase proportions for each experiment are given in Table 1.

3.1. Melt compositions

Bulk composition 0 wt.% S: there was one melt in equilibrium with cohenite at 1150 °C at each pressure (3 and 6 GPa) of the experiments; the melt compositions are different at 3 and 6 GPa. There was no graphite produced in either sample (Fig. 1). The liquid in equilibrium with cohenite was rich in Fe–C–Ni with the Ni and C content increasing as pressure increased at the expense of Fe.

Bulk composition 4.7 wt.% S: At 3 GPa and 1150 °C this composition shows an S-rich liquid, cohenite, and an enigmatic intergrowth of cohenite and Fe-alloy (TT-733, Fig 1). This intergrowth at the cold end of the charge is S-free, presumably therefore not in equilibrium with the rest of the charge, and is not considered further. The hot-end liquid was sulfur-rich and in major element content quite similar to the sulfur-rich liquids from our other experiments. At 6 GPa and 1150 °C, besides cohenite, only S-rich liquid phase was present. The Fe-bearing solid in all experiments at this bulk composition was cohenite (Fig. 1).

Bulk composition 14 wt.% S: at 3 GPa this composition showed one liquid phase and one crystal phase (cohenite). At 6 GPa there were two crystalline phases (cohenite, graphite) and one liquid phase (Fig. 1) (Table 1).

Table 2
Composition of the experimental phases

Run No.	B.C. 89.62 wt.% Fe–4.72 wt.% C–5.23 wt.% Ni–0.43 wt.% trace				B.C. 84.9 wt.% Fe–4.72 wt.% S–4.72 wt.% C–5.23 wt.% Ni–0.43 wt.% trace				B.C. 75.47 wt.% Fe–14.15 wt.% S–4.72 wt.% C–5.23 wt.% Ni–0.43 wt.% trace			
	TT-731	TT-731	TT-716	TT-716	TT-733	TT-733	TT-726	TT-726	TT-728	TT-728	BB-965	BB-965
P (GPa)	3	3	6	6	3	3	6	6	3	3	6	6
n[a] EPMA C/Al coat	19/29	6/50	19/39	21/39	18/40	23/65	21/48	21/45	20/30	21/52	24/18	53/34
n[b] LA-ICP-MS	4	7	2	6	5	3	3	4	5	5	3	7
Phase	Fe_3C	Liquid	Fe_3C	Liquid	Fe_3C	Liquid S	Fe_3C	Liquid	Fe_3C	Liquid	Fe_3C	Liquid
Fe (wt.%)	91.8	89.1	88.9	86.8	90.1	67.9	89.9	70.1	90.3	65.8	90.1	67.5
1σ	1.2	0.7	1.3	0.8	0.5	1	1.6	0.9	2.2	1.7	1.3	1
Ni (wt.%)	2.3	6.4	3	7.2	2.4	8.2	2	8.2	2.3	8.5	2.4	9.2
1σ	0.5	0.8	0.8	0.7	0	0.5	0.2	0.3	0.1	0.5	0	0.5
C (wt.%)	5.5	4	7	5.6	7	1.9	7.6	4.6	6.1	2.6	6.5	3.2
1σ	0.8	0.7	0.7	0.9	0.6	0.7	2.1	1.6	0.5	1.2	1.6	0.8
S (wt.%)	0	0	0	0	0	21.8	0	17.1	0.1	22.7	0	21.8
1σ	0	0	0	0	0.1	1.1	0	0.6	0.2	0.6	0	0.8
Co (ppm)	350	690	370	1340	670	530	630	840	1830	1710	950	1470
1σ	240	66	210	88	13	51	33	110	48	130	26	51
Os (ppm)	360	710	340	820	480	32	410	160	1010	70	960	100
1σ	69	60	2	110	15	5	48	22	25	6	200	12
Pt (ppm)	20	260	28	400	29	110	20	340	250	1330	10	160
1σ	16	30	2	43	5	10	2	45	18	160	1	15
Re (ppm)	550	690	470	780	520	17	370	52	800	20	940	29
1σ	63	98	2	120	81	3	37	7	35	3	210	3
W (ppm)	420	660	540	710	520	22	310	61	640	23	230	75
1σ	69	96	2	34	58	3	69	5	26	2	14	9
Total	99.8	99.9	99.0	100.0	99.7	99.9	99.8	99.7	100.2	99.3	99.9	99.4

Fe, C, Ni, and S (reported in wt.%) were measured by electron microprobe. Trace elements (reported in ppm) were measured by LA-ICP-MS. 1σ Uncertainties are based on replicate analyses.

[a] Number of electron probe spots analyses used to obtain the reported major element concentrations the first number is the number of spots conducted while the samples were carbon coated the second number is the number of spots conducted while the samples were Al coated.

[b] Number of LA-ICP-MS spot analyses used to obtain the reported trace element concentrations.

4. DISCUSSION

This study explored the effect of light element content (S specifically) of carbon-bearing liquid in controlling the partitioning when the solid is cohenite instead of crystalline Fe. Ni partitioning into cohenite exhibits some curious behavior compared to its partitioning into Fe metal as do some of the other siderophile elements. In Figs. 2–4 the elements are ordered by increasing *D* in the Fe–S system, based upon literature data (Chabot et al., 2007; Van Orman et al., 2008; Stewart et al., 2009) at 32 mol.% S in the liquid. This value of S was chosen because it is the lowest value with data available for W and it is a midpoint for most of the other elements in in the Fe–S data sets (Fig. 3). Any dip in the pattern reflects a departure from *D* behavior in the Fe–S system. In this section we compare our results with those of previous studies on the Fe–S (Chabot et al., 2007; Van Orman et al., 2008; Stewart et al., 2009) and Fe–C (Chabot et al., 2006, 2008) systems (Fig. 3).

4.1. Phases present

Cohenite is the crystalline phase in all the experiments we report here at 1150 °C in Fe–Ni–S–C at 6 GPa. However, previous work (Dasgupta et al., 2009) showed that Fe_7C_3 is the stable phase in the Fe–S–C system at 1150 °C and 15 wt.% S in the starting bulk composition. These conditions are the same as those of BB-965 (Table 1), except the current experiments contain Ni. The addition of Ni increases the stability of cohenite over Fe_7C_3 and destabilizes the solvus to lower temperatures for higher bulk S content. By staying in the field of cohenite phase stability at variable *P* we were able to avoid the added complication of a phase substitution of a different carbide.

4.2. Effect of sulfur on partitioning at a fixed *P*

At 3 GPa the liquids at both 4.7 wt.% S and 14 wt.% S starting compositions are close to 31 mol.% S. Their *D*s are also indistinguishable. At 3 GPa a variation of 10 wt.% S in the starting composition has no noticeable effect on the liquid composition or the measured *D*s. D_{Os}, D_{Re}, and D_W for cohenite–S-rich metallic melt are at least an order of magnitude greater than the cohenite/C-rich, S-free melt *D*s. This indicates that the presence of S has a large effect on some of the *D*s in the Fe–Ni–S–C system at 3 GPa (Fig. 2, Table 3).

At 6 GPa, variability in *D*s can be characterized by the S content of the liquid. Unlike at 3 GPa, the S content of the liquid composition changes from 24 mol.% to ~29 mol.%

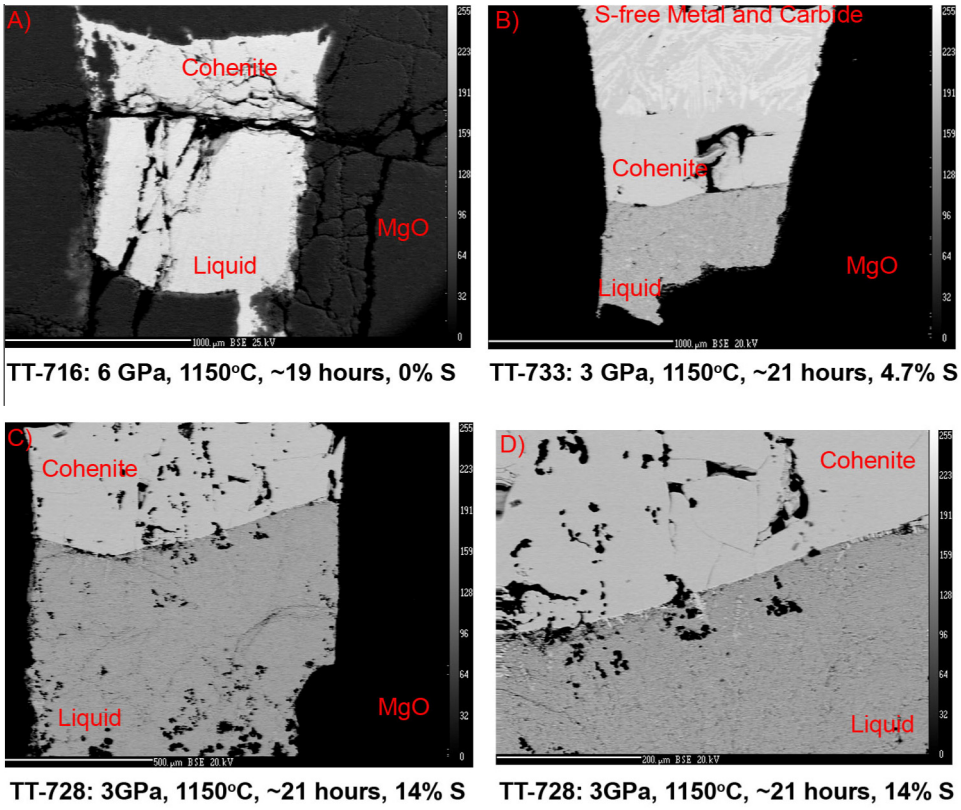

Fig. 1. Representative back-scattered electron images of the experimental products in MgO capsules. All experiments were homogenized at 1400 °C before being dropped to run temperature of 1150 °C. (A) TT-716: The lower portion of this experiment is a C-rich liquid while the upper portion is cohenite. This charge is representative of the textures seen in both the 3 GPa (TT-731) and 6 GPa (TT-716) experiments where S was absent. The clean separation of the phases that facilitates their well-differentiated, separate analysis is caused by thermal compaction in the small temperature gradient within the charge. The direction of thermal migration separation, putting cohenite in the cold region of the charge, indicates that the cohenite becomes less soluble in the liquid as temperature falls. (B) TT-733: This experiment presents three zones of product. Moving from the bottom up from hotter to colder in the charge: the S-rich liquid; cohenite; and an occluded region in which sprays of essentially S-free metal and carbide coexist. The compositions reported for this study are those of the cohenite from the middle zone and the quenched liquid from the lower zone. The region of occluded cohenite–metal sprays does not appear to participate in the liquid–cohenite thermal compaction equilibrium which is the subject of this study. (C and D) TT-728: Shows the sulfide-rich quenched metallic melt at the bottom of the image, composed of sulfide matte with dendrites of metallic iron, coexisting with cohenite, at the top of the image. This charge, like BB-965, is graphite-saturated in both the liquid and solid phase. (D) is a close-up of the crystal–liquid interface.

Table 3
Partition coefficients

Run	Phase	P (GPa)	S + C	D_{Ni}	1σ	D_{Co}	1σ	D_{Os}	1σ	D_{Pt}	1σ	D_{Re}	1σ	D_{W}	1σ
TT-731	Fe_3C/liquid	3	17	0.36	0.15	0.51	0.44	0.51	0.15	0.08	0.08	0.79	0.24	0.64	0.23
TT-716	Fe_3C/liquid	6	22	0.41	0.17	0.28	0.19	0.41	0.06	0.07	0.01	0.60	0.12	0.76	0.04
TT-733	Fe_3C/liquid	3	38	0.29	0.02	1.3	0.16	15	3.2	0.26	0.07	31	11	24	6.1
TT-726	Fe_3C/liquid	6	40	0.24	0.03	0.74	0.15	2.6	0.76	0.06	0.02	7.0	2.0	5.1	1.7
TT-728	Fe_3C/liquid	3	41	0.28	0.03	1.1	0.12	14	1.6	0.18	0.04	41	8.3	28	3.6
BB-965	Fe_3C/liquid	6	41	0.27	0.02	0.65	0.04	9.2	3.4	0.07	0.01	33	13	3.0	0.61

(S + C) is in mol.%. D's are calculated by weight. 1σ for D_{Ni}, for instance, calculated from $\{X_{Ni}(Fe_3C) + \text{stdev}[X_{Ni}(Fe_3C)]\}/\{X_{Ni}(\text{liq}) - \text{stdev}[X_{Ni}(\text{liq})]\} - D$. The values of stdev[$X_{Ni}(Fe_3C)$] and stdev[$X_{Ni}$(liq)] are taken from the 1σ values in Table 2 for individual phase analyses.

as the bulk composition increases from 4.7 wt.% S to 14 wt.% S. D_{Co}, D_{Re}, and D_{Os} increase as S content in the liquid increases. D_{Ni} decreases when transitioning from C-rich to S-rich liquid, then remains roughly constant. D_{Pt} and D_{W} remain roughly constant (Fig. 2, Table 3).

4.3. Effect of pressure on partitioning

In the nominally sulfur-free composition there is no noticeable pressure effect on any of the Ds (Fig. 2, Table 3). In the composition with 4.7 wt.% S, increasing pressure

causes a variation in the S content of the liquid. As the S content of the liquid increases, D_{Pt}, D_W, D_{Re} and D_{Os} all increase. D_{Ni} decreases slightly and D_{Co} shows a slight increase, but a lot of the variation for D_{Co} is within error. At this composition there is no P dependence which can be separated from the variation of S in the liquid (Fig. 2, Table 3).

In the 14 wt.% S-bearing composition, graphite is stabilized at 6 GPa but not at 3 GPa. BB-965 and TT-728 have identical S + C values (within error). Since TT-728 is at 3 GPa and BB-965 is at 6 GPa but the S + C values are identical any variation in Ds can be attributed to a P effect. The only Ds which vary between these 2 experiments are D_W and D_{Pt}. At 3 GPa D_W is 28.6 and at 6 GPa D_W is 3.1. The change in D_{Pt} is less but still outside of the analytical error (Fig. 2, Table 3).

4.4. Cohenite vs. Fe-metal

Previously, partitioning behavior in metal-rich systems has been successfully characterized by the fraction of non-metals such as S and P in liquid compositions. It has been suggested that the addition of C could also be accounted for with these models (Jones and Malvin, 1990; Chabot and Jones, 2003; Stewart et al., 2009). In this study we explore the extreme case of C inclusion, when the liquid is no longer in equilibrium with Fe metal but with cohenite. When the light element content of the liquid is the same are the Ds for cohenite and Fe the same? Even if the Ds are different, can the previous models capture the cohenite system behavior or is a new formulation required? To answer these questions we have compiled literature data and plotted it as D vs. light element content of the liquid (Fig. 3). These figures have experimental data over a wide P and T range (Chabot et al., 2006, 2007, 2008; Van Orman et al., 2008; Stewart et al., 2009). P and T appear to have little effect on D as shown in the review of P effects above and previously for crystalline Fe (Jones and Walker, 1991). The behaviors of the log Ds in the Fe–S, Fe–C, and cohenite systems may be characterized by exponential fits to the nonmetal content of the liquid (Fig. 3).

4.4.1. Metallic Fe/S-bearing metallic liquid partitioning vs. cohenite/metallic alloy liquid partitioning

For any given light element concentration in the liquid, going from Fe solid to cohenite solid causes Ds to decrease (Fig. 3) for all elements except W. This difference becomes more pronounced as the light element concentration, i.e., total S + C of the liquid is increased. In the system without C, D increases with increasing light element content (Fleet et al., 1999; Chabot et al., 2003, 2006, 2007, 2008, 2011; Lazar et al., 2004; Van Orman et al., 2008; Walker and Li, 2008; Hayashi et al., 2009; Stewart et al., 2009; Hayden et al., 2011); (Fig. 3). This relationship is also seen when cohenite is the crystalline phase for all elements except Ni. D_{Ni} changes from a positive slope in the D (Fe-metal/C-rich liquid) and D (Fe-metal/S-rich liquid) to a negative slope in the D (cohenite/liquid) plot (Fig. 3). The presence of S in liquid drives Ni into the crystalline metal. It appears that the nonmetal content of cohenite overcomes the effect of S in the liquid and returns Ni behavior to incompatible (Romig and Goldstein, 1980; Cacciamani et al., 2010). This change in behavior must relate to the presence of cohenite, not just the inclusion of C in the liquid, since we do not see a negative slope in the "(S + C) in the liquid vs. D (Fe-metal/C-rich liquid)" data (Chabot et al., 2006; Chen et al., 2008) (Fig. 3).

4.4.2. Metallic Fe–C-bearing metallic liquid partitioning vs. cohenite-metallic alloy liquid partitioning

In the Fe–S vs. cohenite–S-bearing melt system, Ds for most elements decrease when the transition from Fe metal to cohenite is made. This does not appear to be true for W. In the small area of S + C space where experiments have been done in both the Fe-metal–C-bearing liquid and cohenite–liquid systems, D_W are about equal, and if the lower S + C trend in the 'metallic Fe–C-bearing liquid' data set were to continue, D_W would be smaller than in the cohenite–C-bearing liquid system (Fig. 3). Another interesting thing is that D_{Re} and D_W both appear to have a negative slope in the Fe metal–C-bearing liquid system when plotted "(S + C) liquid vs. D". In contrast, they have positive slopes in the cohenite–liquid system, and where D_{Ni} in the cohenite–liquid system has a negative slope it has a positive slope in the Fe-metal–C-bearing liquid system (Fig. 3). The changes in D and the changes of slope in Fig. 3 are not only functions of liquid composition but also depend on the identity of the crystalline phase.

4.5. Models

Fig. 3 demonstrates that D is a function of the non-metal content of the liquid phase (with somewhat different dependencies for different crystalline phases). The successful formulations of D for crystalline Fe metal based on liquid phase composition (Jones and Malvin, 1990; Chabot and Jones, 2003) may have analogs that apply to the Ds for cohenite. The model of Jones and Malvin (1990) supposes that trace elements either avoid or seek the non-metals in the liquid, with the balance being accommodated in the crystal. The site availability in the liquid, not occupied by the non-metals and their associated Fe in whatever species they exist, conditions the extent to which trace elements reside in either liquid or crystal. The strength of the non-metal avoidance is characterized by the interaction parameter between the trace element and the non-metals. It is expected that the interaction parameter for some trace element could be different for Fe and liquid than it is for cohenite and liquid. The following form was suggested by Jones and Malvin (1990) as a possible way to treat more than one non-metal in the liquid, in this case non-metals S and C for the partitioning of Ni.

$$\ln(D_{Ni}) = {}^{Ni}\beta_{sc} \cdot \ln[1 - A_s \cdot \alpha_s \cdot X_s - A_c \cdot \alpha_c \cdot X_c] + \text{Const} \quad (1)$$

${}^{Ni}\beta_{sc}$ is the interaction parameter for Ni with both S and C in the cohenite–liquid equilibrium. A_s and A_c are the stoichiometric factors for the speciation of the non-metal with Fe in the liquid. For example FeS has $A_s = 2$ because two sites are not available for a trace element if they are

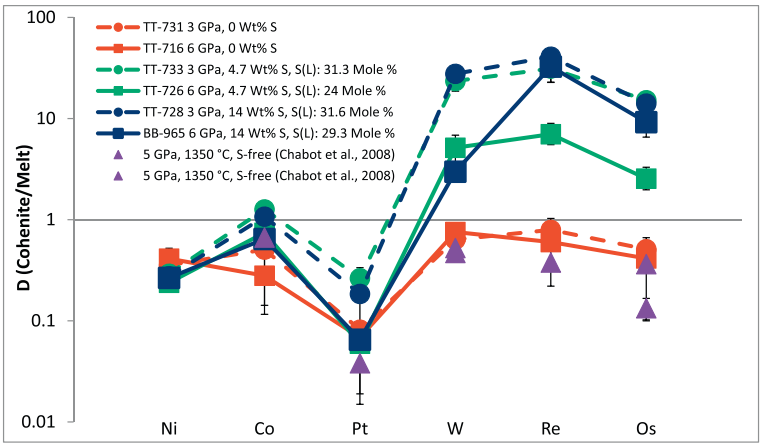

Fig. 2. This figure shows the effect of S variation in the bulk composition as well as the effect of P on D at 3 and 6 GPa. Dashed lines and circles indicate 3 GPa experimental data. Solid lines and squares represent 6 GPa experimental data. Red points contain no S, green are 4.7 wt.% S and blue contained 14 wt.% S in the starting composition. The purple triangles are literature data (Chabot et al., 2008). The sequence of elements along the X-axis is in the order of increasing D for the Fe-metal/alloy melt pairs in the Fe–S system. Every dip in the sequence represents a change in the overall behavior of D between the Fe–S and Fe–Ni–S–C systems, reflecting the change in crystalline phase from iron to cohenite. Cohenite generally accepts less of the siderophile elements than does iron. Pt partitions much less readily into cohenite than into iron than any of the other elements investigated, except Ni in some cases. (For interpretation of the references to colour in this figure legend, the reader is referred to the web version of this article.)

occupied by an Fe and its associated S. α_s and α_c are factors not very different from one that scale the compositional range until eutectic saturation is reached. Thus the argument of the natural log in [ ] is the fraction of sites in the liquid that are not available to hold the element of interest, here Ni. If this form applies to cohenite–liquid partitioning, one should expect that the argument of the natural log in [ ] plotted against the $\ln(D_{Ni})$ should give a line. Taking α_s and α_c as 1 and A_s and A_c as 2, Fig. 4 recasts the data of Fig. 3 into this tentative Jones and Malvin form. (For A_c greater than 2, the argument of the ln[ ] becomes negative, providing a rough cap on the extent of allowed Fe–C associations in the liquid.) It can be seen in Fig. 4 that there is reasonable conformance to linear plots, of variable quality, encouraging the view that cohenite–liquid partitioning behavior pays some attention to non-metal avoidance principles. Linear plots are approximately found also for Co, Pt, W, Re, and Os. The negative slope of the plot for Ni in Fig. 4, in contrast to all the other elements, suggests that the interactions with S and C have some affinity rather than being only ones of avoidance. A more detailed treatment is unwarranted at present, however future investigations may find this framework useful.

4.6. Effect on planetary cores

Cohenite is a possible solid core component in small planets such as Mercury and moons such as Earth's Moon. If cohenite is a major core component, we can expect less severe depletions in all of the elements studied in the liquid outer core relative to the Fe–Ni–S system and less severe depletions in all elements except for W in the Fe–C system where the inner core is Fe. This is especially true for Ni where D changes from greater than 1 when partitioned between an Fe-metal and a metallic liquid to less than one when partitioned between cohenite and a metallic liquid. Given a large amount of cohenite formation, this would lead to Ni enrichment in the liquid outer-core instead of the less severe depletion expected from the Fe–C system when Fe is the crystallizing solid.

4.7. Effect on siderophile element distribution in the Earth's mantle

The partition coefficients between cohenite and Fe–Ni–C±S melts (this study) are significantly lower than those between Fe-metal and S-rich liquid for all of the elements studied here. This is also true for Fe-metal and C-rich liquid (Chabot et al., 2006, 2008), except in the case of Chabot et al. (2008) showed that the Ds for cohenite/liquid were <1 for S-free liquids. We confirm their result and show that it also applies to a wide range of S + C-bearing liquids. The $D < 1$ indicates that in the presence of cohenite and Fe–Ni–C–S liquid in the mantle, the siderophile element budget of the mantle may be preferentially accommodated by Fe–C±S liquid rather than solid Fe-carbide. This is especially true for Ni, Co, and Pt, all of which become moderate to highly incompatible in the solid if cohenite is stable instead of Fe-metal. W, Re, and Os also become slightly enriched in the C-rich Fe–Ni liquid over cohenite if the system is S-free. The depth of transition from cohenite, $(Fe,Ni)_3C$, to $(Fe,Ni)_7C_3$ is not well constrained at present, however, unless the siderophile element partitioning behavior is significantly different between $(Fe,Ni)_7C_3$ and metallic liquid compared to cohenite and liquid, our prediction of siderophile element budget of the mantle being dominated by C±S-bearing metallic liquid will likely hold.

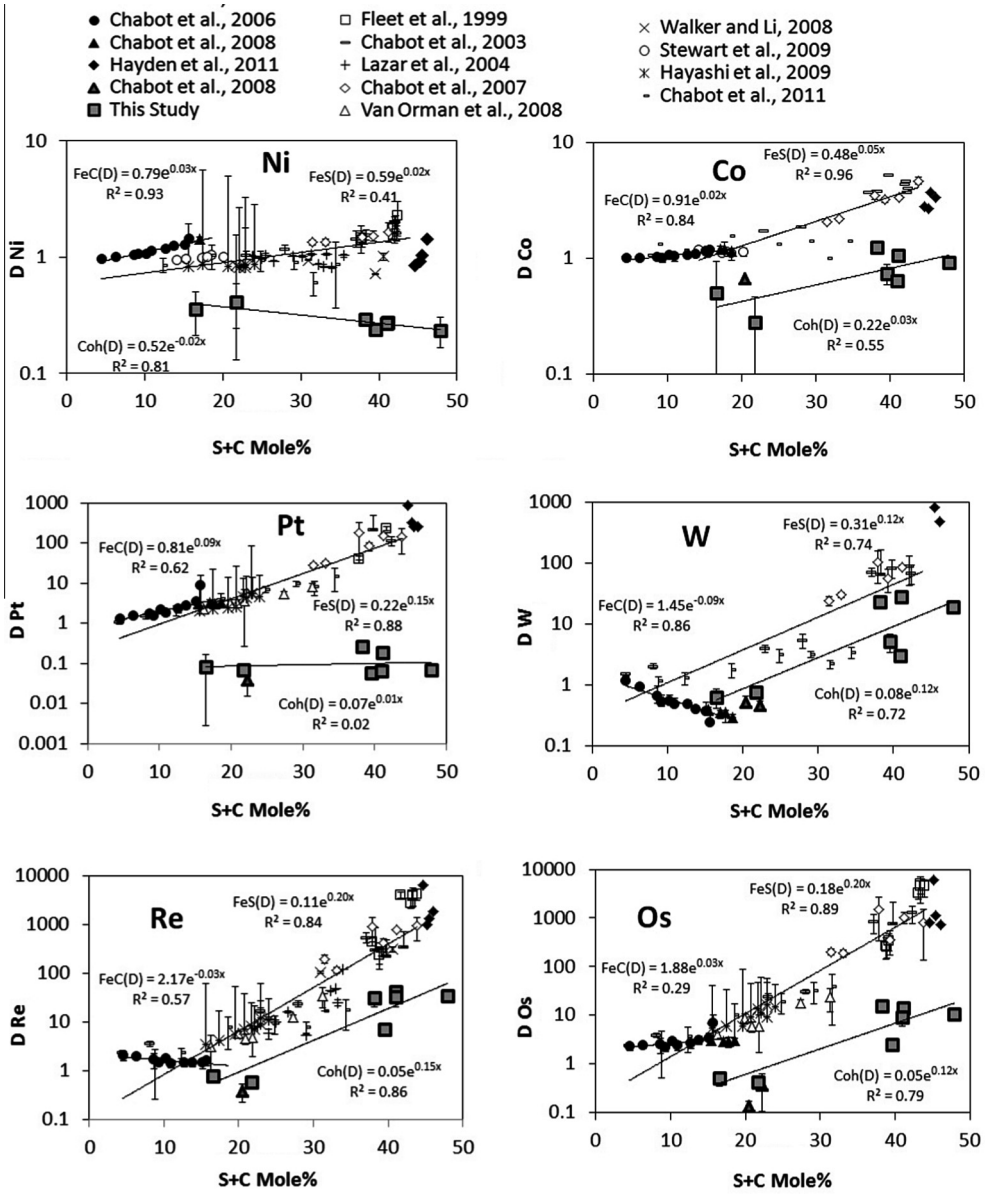

Fig. 3. Plots of crystal/liquid D vs. mol.% of sulfur + carbon in the metallic liquid. These figures have experimental data over a wide P and T range. Despite this large P–T range it is possible to fit each data set with an exponential function with liquid composition alone as the independent variable, indicating the importance of liquid composition (more than T or P) in determining cohenite–liquid siderophile element partitioning. Unfilled shapes and dashes represent data from literature studies on both the Fe–Ni–S and Fe–S systems (Fleet et al., 1999; Chabot et al., 2003, 2007, 2011; Lazar et al., 2004; Van Orman et al., 2008; Walker and Li, 2008; Hayashi et al., 2009; Stewart et al., 2009; D written as 'FeS(D)'). The thick walled squares and triangles with grey interiors represent data from the Fe–C–S and Fe–Ni–C–S systems where cohenite is the crystalline phase (This study; Chabot et al., 2008; D written as 'Coh(D)'). The filled circles and triangles represent data from the Fe–C and Fe–Ni–C systems where Fe is the crystalline phase (Chabot et al., 2006, 2008; Hayden et al., 2011; D written as 'FeC(D)'). Hayden et al. (2011) values are plotted but not included in calculating the trend lines since these experiments contain C in the crystalline Fe but not in the liquid.

4.8. The effect of cohenite on the coupled enrichment in Pt, Re, and Os in outer core liquid

Previous work has suggested that material transfer from the Earth's outer core to the base of the mantle has led to a coupled enrichment in the $^{186}Os/^{188}Os$ (Pt/Os) and $^{187}Os/^{188}Os$ (Re/Os) system in some ocean island basalts (Brandon and Walker, 2005; Walker et al., 2005). Later work on siderophile element partitioning between metallic-Fe and melt in the Fe–FeS system indicated that it is not possible to recreate these anomalies at reasonable S contents of the metallic melt (Van Orman et al., 2008). Even though it is unlikely that the core of Earth is pure cohenite, our study provides a useful opportunity to look at the effect

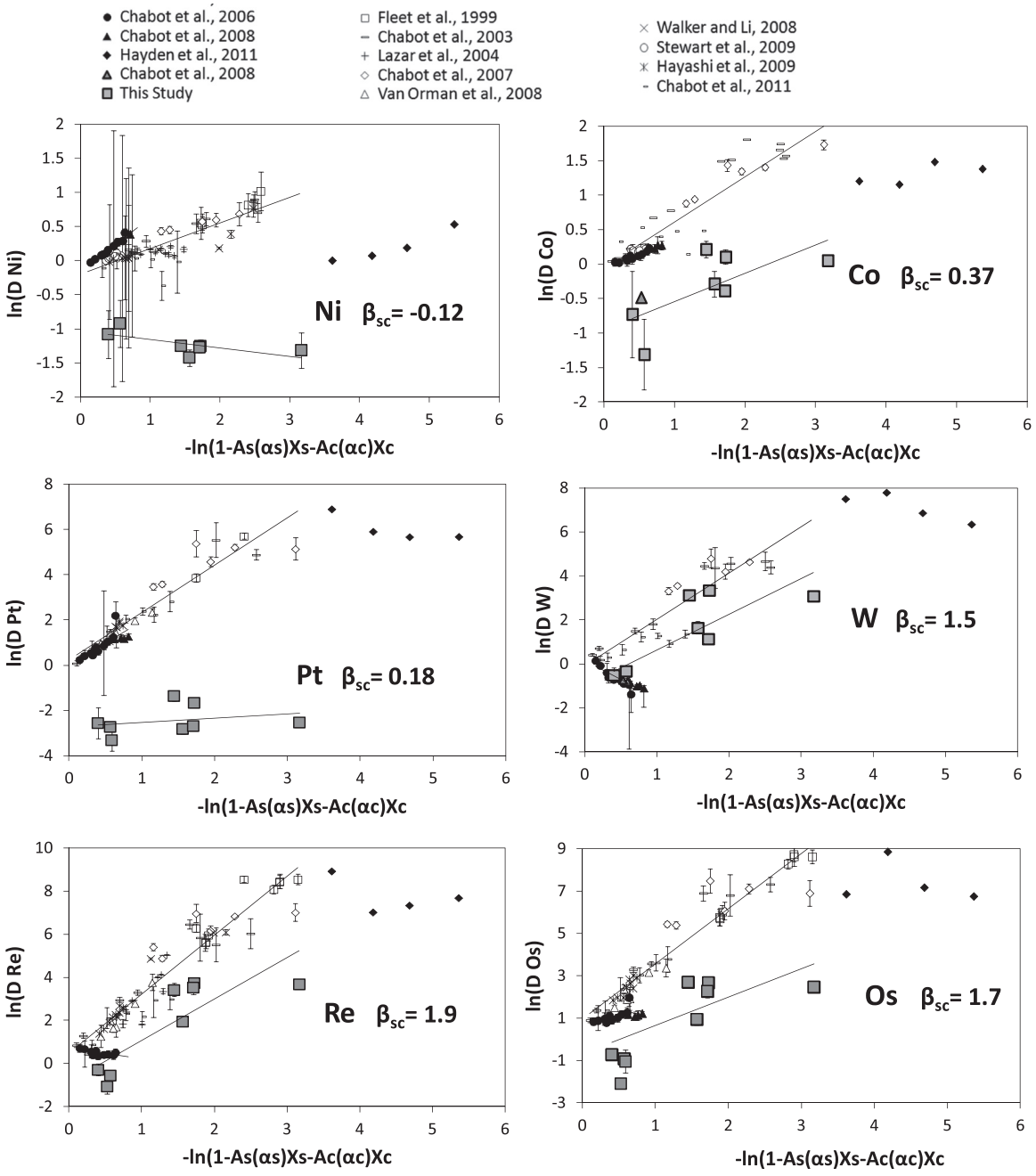

Fig. 4. The data of Fig. 3 are recast into Jones and Malvin (1990) form. The symbols for data sources are the same as in Fig. 3. The *A*s and *A*c stoichiometric factors for sulfur and carbon species are set to 2, whereas the α factors are set to 1. The β_{SC} values are the slopes of the cohenite partitioning data arrays.

that moving from Fe crystallization to cohenite crystallization has on D_{Pt}, D_{Os}, and D_{Re}. Thus we can evaluate whether cohenite crystallization in the inner core helps explain the coupled enrichment of Pt–Os and Re–Os system in the outer core liquid. Using the most favorable case, where the inner core attained its present mass (~5.5% of the entire core) just after formation, i.e., between 4.4 and 4.3 Ga and by pure fractional crystallization process, the Pt/Os and Re/Os ratio of the outer core liquid are given by

$$(\mathrm{Pt/Os})_{\text{outer core}} = F({}^{D}\mathrm{Pt} - {}^{D}\mathrm{Os}) \quad (2)$$

$$(\mathrm{Re/Os})_{\text{outer core}} = F({}^{D}\mathrm{Re} - {}^{D}\mathrm{Os}) \quad (3)$$

where F is the mass fraction of outer core liquid. Eqs. (2) and (3) above give the maximum possible isotopic ratios of $^{187}Re/^{188}Os$ and $^{190}Pt/^{188}Os$ in the outer core liquid, set early in the Earth's history and thus provide the best case scenario for coupled enrichment of $^{186}Os/^{188}Os$ and $^{187}Os/^{188}Os$. To match the observed enrichment in OIB la-

vas, (D_{Pt}–D_{Os}) and (D_{Re}–D_{Os}) values are required to be ~−25 and −10, respectively (Van Orman et al., 2008).

By using the exponential fits for the cohenite–liquid metal system shown in Fig. 3, and for the metallic liquid composition ranging from 15 to 50 mol.% S + C, we obtain the (D_{Pt}–D_{Os}) and (D_{Re}–D_{Os}) values of −0.1 to −26.8 and 0.14–65.1. Hence, we conclude that although it is possible to match the requirement of (D_{Pt}–D_{Os}) of ~−25, cohenite crystallization produces an opposite effect to what is required to obtain the (D_{Re}–D_{Os}) value. Furthermore, even to match the (D_{Pt}–D_{Os}) of ~−25, a metallic liquid with S + C content of 49.5 mol.% is required, which is unrealistically high. Thus our analysis suggests that crystallization of pure cohenite inner core does not result in the coupled enrichment seen in some ocean island lavas. Hence our data do not support cohenite as a possible remediant to the difficulties in the evidence for core–mantle interaction.

5. CONCLUSION

The transition of the crystalline phase from metallic Fe to cohenite causes first-order changes in the partition coefficients in the elements studied. This change causes the previous solidification models for Fe (Jones and Malvin, 1990; Chabot and Jones, 2003), to no longer be quantitatively predictive. However, we still find that light element (S + C) content of the liquid is the most important controlling factor in partitioning as in those previous models for Fe. Varying pressure from 3 to 6 GPa has no noticeable effect in the S-rich system except for D_W. The most unanticipated result of this research is the shift from a D greater than 1 in the Fe-liquid system for Ni, Co, and Pt to a D less than 1 in the cohenite–liquid system. In hindsight this is probably non-metal avoidance in the crystal. As C is put into the crystal forming cohenite the siderophile elements are preferentially excluded. It appears that the presence of C in the solid overcomes the effect of S in the liquid and returns Ni behavior to incompatible.

Given that the partition coefficients between cohenite and Fe–C±S melts for all the elements studied here are significantly lower than those between Fe-metal and liquid, we predict that in the presence of cohenite in the Earth's mantle or the core of smaller planets there would be a less severe depletion in the coexisting liquid for all of the elements studied, relative to the Fe-metal-sulfide liquid and Fe-metal (dissolved C)-carbon-bearing metallic liquid systems. The enrichment of the coexisting liquid over cohenite is especially true for Ni, Co, and Pt, all of which become moderate to highly incompatible if the solid of interest is cohenite rather than Fe-metal.

ACKNOWLEDGEMENTS

R.D. received support from a Packard Fellowship. D.W., A.B., and C.L. received support from NSF. We thank N. Chabot and two anonymous reviewers for their comments and N. Chabot for sharing her literature data base of D values.

REFERENCES

Agranier A. and Lee C.-T. A. (2007) Quantifying trace element disequilibria in mantle xenoliths and abyssal peridotites. *Earth Planet. Sci. Lett.* **257**, 290–298.

Anderson O. L. and Isaak D. G. (2002) Another look at the core density deficit of Earth's outer core. *Phys. Earth Planet. Inter.* **131**, 19–27.

Bild, R.W., Drake, M.J., 1978. Experimental investigations of trace element fractionation in iron meteorites. I-Early results, Lunar and Planetary Science Conference, 9th, Houston, Tex.

Birch F. (1952) Elasticity and constitution of the Earth's interior. *J. Geophys. Res.* **57**, 227–286.

Brandon A. D. and Walker R. J. (2005) The debate over core–mantle interaction. *Earth Planet. Sci. Lett.* **232**, 211–225.

Brett R. and Bell P. M. (1969) Melting relations in the Fe-rich portion of the system Fe–FeS at 30 kb pressure. *Earth Planet. Sci. Lett.* **6**, 479–482.

Buchwald V. F. (1975) *Handbook of Iron Meteorites. Their History, Distribution, Composition and Structure*. University of California Press, Berkeley, Los Angeles, London.

Buono A. S. and Walker D. (2011) The Fe-rich liquidus in the Fe–FeS system from 1 bar to 10 GPa. *Geochim. Cosmochim. Acta* **75**, 2072–2087.

Cacciamani G., Dinsdale A., Palumbo M. and Pasturel A. (2010) The Fe–Ni system: thermodynamic modelling assisted by atomistic calculations. *Intermetallics* **18**, 1148–1162.

APPENDIX 1

Other runs that were conducted during this study. These lacked a homogenization step and had run temperatures which placed them beyond the scope of this study.

Run No.	P (GPa)	T (°C)	Duration in hours	Bulk composition of the starting material	Phase assemblage and proportion
BB-937	6	1150	26.15	75.47 wt.% Fe; 4.72 wt.% C; 14.15 wt.% S; 5.23 wt.% Ni; 0.43 wt.% Trace	70% Liquid + 30% Cohenite + Trace Graphite
BB-935	6	1250	50.63	75.47 wt.% Fe; 4.72 wt.% C; 14.15 wt.% S; 5.23 wt.% Ni; 0.43 wt.% Trace	Liquid + Graphite
BB-934	6	1250	47.3	84.9 wt.% Fe; 4.72 wt.% C; 4.72 wt.% S; 5.23 wt.% Ni; 0.43 wt.% Trace	Liquid + 82 mol.% Fe carbide
TT-713	6	1352	20.4	89.62 wt.% Fe; 4.72 wt.% C; 5.23 wt.% Ni; 0.43 wt.% Trace	95% Liquid + 5% Cohenite
TT-712	6	1450	5.45	89.62 wt.% Fe; 4.72 wt.% C; 5.23 wt.% Ni; 0.43 wt.% Trace	100% Liquid

Campbell A. J. and Humayun M. (2005) Compositions of group IVB iron meteorites and their parent melt. *Geochim. Cosmochim. Acta* **69**, 4733–4744.

Chabot N. L. and Jones J. H. (2003) The parameterization of solid metal–liquid metal partitioning of siderophile elements. *Meteorit. Planet. Sci.* **38**, 1425–1436.

Chabot N. L., Campbell A. J., Jones J. H., Humayun M. and Agee C. B. (2003) An experimental test of Henry's Law in solid metal–liquid metal systems with implications for iron meteorites. *Meteorit. Planet. Sci.* **38**, 181–196.

Chabot N. L., Campbell A. J., Jones J. H., Humayun M. and Lauer, Jr., H. V. (2006) The influence of carbon on trace element partitioning behavior. *Geochim. Cosmochim. Acta* **70**, 1322–1335.

Chabot N. L., Saslow S. A., McDonough W. F. and McCoy T. J. (2007) The effect of Ni on element partitioning during iron meteorite crystallization. *Meteorit. Planet. Sci.* **42**, 1735–1750.

Chabot N. L., Campbell A. J., McDonough W. F., Draper D. S., Agee C. B., Humayun M., Watson H. C., Cottrell E. and Saslow S. A. (2008) The Fe–C system at 5 GPa and implications for Earth's core. *Geochim. Cosmochim. Acta* **72**, 4146–4158.

Chabot N. L., McDonough W. F., Jones J. H., Saslow S. A., Ash R. D., Draper D. S. and Agee C. B. (2011) Partitioning behavior at 9 GPa in the Fe–S system and implications for planetary evolution. *Earth Planet. Sci. Lett.* **305**, 270–282.

Chen B., Li J. and Hauck S. A. (2008) Non-ideal liquidus curve in the Fe–S system and Mercury's snowing core. *Geophys. Res. Lett.* **35**, L07201–L07201.

Dasgupta R. and Hirschmann M. M. (2010) The deep carbon cycle and melting in Earth's interior. *Earth Planet. Sci. Lett.* **298**, 1–13.

Dasgupta R. and Walker D. (2008) Carbon solubility in core melts in a shallow magma ocean environment and distribution of carbon between the Earth's core and the mantle. *Geochim. Cosmochim. Acta* **72**, 4627–4641.

Dasgupta R., Buono A., Whelan G. and Walker D. (2009) High-pressure melting relations in Fe–C–S systems: Implications for formation, evolution, and structure of metallic cores in planetary bodies. *Geochim. Cosmochim. Acta* **73**, 6678–6691.

Dasgupta R., Chi H., Shimizu N., Buono A. S. and Walker D. (2013) Carbon solution and partitioning between metallic and silicate melts in a shallow magma ocean: implications for the origin and distribution of terrestrial carbon. *Geochim. Cosmochim. Acta* **102**, 191–212.

Dasgupta R. (2013) Ingassing, storage, and outgassing of terrestrial carbon through geologic time. *Rev. Mineral. Geochem.* **75**, 183–229.

Fei Y., Bertka C. M. and Finger L. W. (1997) High-pressure iron–sulfur compound, Fe_3S_2, and melting relations in the Fe–FeS system. *Science* **275**, 1621–1621.

Fleet M. E., Liu M. and Crocket J. H. (1999) Partitioning of trace amounts of highly siderophile elements in the Fe–Ni–S system and their fractionation in nature. *Geochim. Cosmochim. Acta* **63**, 2611–2622.

Frost D. J., Liebske C., Langenhorst F., McCammon C. A., Tronnes R. G. and Rubie D. C. (2004) Experimental evidence for the existence of iron-rich metal in the Earth's lower mantle. *Nature* **428**, 409–412.

Hayashi H., Ohtani E., Terasaki H. and Ito Y. (2009) The partitioning of Pt–Re–Os between solid and liquid metal in the Fe–Ni–S system at high pressure: implications for inner core fractionation. *Geochim. Cosmochim. Acta* **73**, 4836–4842.

Hayden L. A., Orman Van., James A., McDonough William F., Ash Richard D. and Goodrich C. A. (2011) Trace element partitioning in the Fe–S–C system and its implications for planetary differentiation and the thermal history of ureilites. *Geochim. Cosmochim. Acta* **75**, 6570–6583.

Jones J. H. and Malvin D. J. (1990) A nonmetal interaction model for the segregation of trace metals during solidification of Fe–Ni–S, Fe–Ni–P, and Fe–Ni–SP alloys. *Metall. Mater. Trans. B* **21**, 697–706.

Jones J. H. and Walker D. (1991) Partitioning of siderophile elements in the Fe–Ni–S system: 1 bar to 80 kbar. *Earth Planet. Sci. Lett.* **105**, 127–133.

Labrosse S. (2003) Thermal and magnetic evolution of the Earth's core. *Phys. Earth Planet. Inter.* **140**, 127–143.

Lazar C., Walker D. and Walker R. J. (2004) Experimental partitioning of Tc, Mo, Ru, and Re between solid and liquid during crystallization in Fe–Ni–S. *Geochim. Cosmochim. Acta* **68**, 643–651.

Lord O. T., Walter M. J., Dasgupta R., Walker D. and Clark S. M. (2009) Melting in the Fe–C system to 70 GPa. *Earth Planet. Sci. Lett.* **284**, 157–167.

McDonough W. F. (2003) Compositional model for the Earth's core. In *Treatise on Geochemistry* (eds. H. D. Holland and K. K. Turekian). Pergamon, Oxford, pp. 547–568.

Morard G., Sanloup C., Fiquet G., Mezouar M., Rey N., Poloni R. and Beck P. (2007) Structure of eutectic Fe–FeS melts to pressures up to 17 GPa: implications for planetary cores. *Earth Planet. Sci. Lett.* **263**, 128–139.

Ono S. and Mibe K. (2010) Magnetic transition of iron carbide at high pressures. *Phys. Earth Planet. Inter.* **180**, 1–6.

Poirier J.-P. (1994) Light elements in the Earth's outer core: a critical review. *Phys. Earth Planet. Inter.* **85**, 319–337.

Rohrbach A., Ballhaus C., Golla-Schindler U., Ulmer P., Kamenetsky V. S. and Kuzmin D. V. (2007) Metal saturation in the upper mantle. *Nature* **449**, 456–458.

Rohrbach A., Ballhaus C., Ulmer P., Golla-Schindler U. and Schönbohm D. (2011) Experimental evidence for a reduced metal-saturated upper mantle. *J. Petrol.* **52**, 717–731.

Romig A. D. and Goldstein J. I. (1980) Determination of the Fe–Ni and Fe–Ni–P phase diagrams at low temperatures (700 to 300 C). *Metall. Trans. A* **11**, 1151–1159.

Stewart A. J., van Westrenen W., Schmidt M. W. and Günther D. (2009) Minor element partitioning between fcc Fe metal and Fe–S liquid at high pressure: the role of crystal lattice strain. *Earth Planet. Sci. Lett.* **284**, 302–309.

Usselman T. (1975) Experimental approach to the state of the core: Part I. The liquidus relations of the Fe-rich portion of the Fe–Ni–S system from 30 to 100 kb. *Am. J. Sci.* **275**, 278–290.

Van Orman J. A., Keshav S. and Fei Y. (2008) High-pressure solid/liquid partitioning of Os, Re and Pt in the Fe–S system. *Earth Planet. Sci. Lett.* **274**, 250–257.

Walker Davi and Li J. (2008) Partitioning of molybdenum to 60 kbar along a warped Fe–FeS liquidus. *Chem. Geol.* **248**, 166–173.

Walker R. J., Brandon A. D., Bird J. M., Piccoli P. M., McDonough W. F. and Ash R. D. (2005) 187Os-186Os systematics of Os–Ir–Ru alloy grains from southwestern Oregon. *Earth Planet. Sci. Lett.* **230**, 211–226.

Walker D., Lord O. T., Walter M. J. and Clark S. M. (2009) X-ray absorption contrast images of binary chemical reactions. *Chem. Geol.* **260**, 211–220.

Wood B. J. and Halliday A. N. (2010) The lead isotopic age of the Earth can be explained by core formation alone. *Nature* **465**, 767–770.

Wood B. J. (1993) Carbon in the core. *Earth Planet. Sci. Lett.* **117**, 593–607.

Associate editor: Richard J. Walker